COMPARISON OF MODIS SNOW ALBEDO TO FIELD MEASUREMENTS IN CENTRAL GREENLAND

A Thesis Presented to

the Faculty of the Department of Earth and Atmospheric Sciences

University of Houston

In Partial Fulfillment

of the Requirements for the Degree

Master of Science

By

Patrick Joseph Wright

May 2012

COMPARISON OF MODIS SNOW ALBEDO TO FIELD MEASUREMENTS IN CENTRAL GREENLAND

Patrick Joseph Wright

APPROVED:

Dr. Barry Lefer, Chairman

Dr. Xun Jiang

Dr. Jack Dibb

University of New Hampshire

Dr. Mark A. Smith

Dean, College of Natural Sciences and Mathematics

ACKNOWLEDGEMENTS

This thesis is dedicated to my father, Lynn C. Wright. He passed away less than two months before the completion of this work, but I am sure that he is proud of the accomplishment. He would have enjoyed to sit down and carefully read through it, despite knowing very little of the topic. From my Dad I learned how to observe the weather, how to think critically and read carefully, and most of all how to communicate my findings to others.

I also very much want to thank my mother, Ann Wright. She started me down the path of being passionate and aware of the natural world at a young age, and encouraged my initial "fieldwork" as I drew sketches and made observations in journals. I was very lucky to learn reading and writing from such a great teacher, and this thesis owes much to the learning I did when I was six and seven years old. The same is true for the many hundreds of other first grade students that learned these essential skills from Ann.

My brother Brad Jaeckel and his family have been a huge source of support, encouragement, and laughter, reminding me of the cooler temperatures and open spaces further north while I lived in Houston.

Much thanks to my advisor, Barry Lefer, who took me on and energetically got me involved in Arctic research, despite being very busy with air quality measurements and many projects closer to home in Houston. I'm lucky to have learned from such a sharp and insightful scientist, who is also a very good person and friend.

This project was a very collaborative effort, and I owe a huge amount of gratitude to everyone that contributed. Jack Dibb at the University of New Hampshire always gave great

comments and insight in reply to almost every question, and brought an amazing amount of Greenland experience to the project. Mike Bergin at Georgia Tech was also a constant source of energy and direction towards the campaign goals, and provided excellent company on the icesheet. Florent Domine and Carlo Carmagnola, with LGGE in France, brought an essential European element to the Summit experience, and both taught me a lot about snow! Also, huge thanks to Marie Dumont at CNRM - France for helping me tackle modeling and albedo correction problems. At Summit Station, Brandon Strellis, Ryan Schilling, Chelsea Corr, and Hannah James operated the ASD instrument to keep our daily measurements going. Thanks to Zoe Courville and Don Perovitch at the CRREL labs in Hanover, New Hampshire, who donated use of the ASD instrument. Everyone at Summit missed Zoe and her snow expertise, so hopefully I was an adequate substitute! Tobey Carman at University of Alaska Fairbanks wrote a very nice piece of code to calculate the weighted integrals which produced the entire albedo dataset for this thesis. Jimmy Flynn at the University of Houston constantly put down his tools while modifying or repairing yet another Thermo box to help me with problems, and Xun Jiang always had an open door for advice on some of the technical and mathematical aspects of my project. Crystal Schaaf and Zhuosen Wang at Boston University dedicated much time to producing the MODIS product and attempted to educate me on the basics of remote sensing. Thanks also to Howard Rodstein at Wavemetrics for awesome customer support throughout my graduate work.

COMPARISON OF MODIS SNOW ALBEDO TO FIELD MEASUREMENTS IN CENTRAL GREENLAND

A Thesis Presented to

the Faculty of the Department of Earth and Atmospheric Sciences

University of Houston

In Partial Fulfillment

of the Requirements for the Degree

Master of Science

By

Patrick Joseph Wright

May 2012

ABSTRACT

Spectral snow albedo, physical snow properties, and snow chemistry were measured daily during May, June, and July 2011 at Summit, Greenland to investigate the variability in snow albedo and its impact on aerosol direct radiative forcing. In this study we compare our spectral albedo measurements to the Moderate Resolution Imaging Spectrometer (MODIS) daily albedo product. We additionally compare to albedo measurements from the Baseline Surface Radiation Network station at Summit (BSRN), and to modeled albedo using measured snow physical and chemical properties as input to the DISORT code. The spectral albedo measurements were made with an Analytical Spectral Devices (ASD) spectroradiometer at 350 – 2200 nm. We calculate weighted integrals of the spectral data to compare to seven MODIS narrow bandwidths ranging the UV through Infrared, as well as a broadband product that represents the full solar spectrum.

Root mean square error (RMSE) for MODIS and field-measured albedo is 0.033 (mean difference of 0.023) for the broadband integration using MODIS high-quality only retrievals, and the narrow bandwidths range 0.022 – 0.077 RMSE (0.009 – 0.063 mean difference). The broadband values show an improvement in error from previous MODIS field validation studies, particularly in the UV and visible wavelengths. MODIS is consistently lower in magnitude than the field measured albedo, and shows poor correlation. The daily and multiday range of variability of the field measurements is much greater than MODIS albedo, and evidence is presented in support of the field-measured daily variability. Spatial variability is also constrained with data from multiple spatial surveys, and it is shown that surface roughness and error due to apparent albedo likely has a dominating effect on spatial variability, whereas the greater range of daily variability is dominated by changes in snow surface properties.

TABLE OF CONTENTS

1. INTRODUCTION

Spectral snow albedo, physical snow properties, and snow chemistry were measured during May, June, and July 2011 at Summit, Greenland to investigate the variability in snow albedo and its impact on aerosol direct radiative forcing. We compare our spectral albedo measurements to the Moderate Resolution Imaging Spectrometer (MODIS) daily albedo product, both to validate the MODIS product, and to investigate the potential for measuring snow surface properties from satellite platforms. The field albedo measurements were made with an Analytical Spectral Devices (ASD) spectroradiometer at 350 – 2200 nm.

Surface albedo is a key parameter needed to estimate the direct radiative forcing by aerosols. Light absorbing black carbon aerosols from biomass burning and fossil fuel combustion, as well as dust, can influence Arctic climate directly by absorbing solar radiation, and can modify the snow surface albedo after deposition. The IPCC attributes a global, annual average net negative radiative forcing due to aerosols of -0.6 W/m^2 to -2.0 W/m^2 (*IPCC,2007)*; however over central Greenland estimates show an instantaneous top of atmosphere radiative forcing of ~10 W/m^2 (a net *positive* forcing), with instantaneous forcing values occasionally reaching 25 W/m^2*(Strellis,2011)*.The variability in surface albedo measured at Summit during our campaign can account for 0.5 – 1.0 W/m^2 of direct radiative forcing *(Strellis, 2011)*; thus the albedo measurements are essential to constrain the magnitude of the forcing.

In addition to radiative forcing by aerosols, accurate measurement of snow albedo variability is important to assess long term changes in planetary albedo, which will be among the most powerful feedback processes in the response of the climate system to anthropogenic forcing. Although the majority of the present global average planetary albedo is due to

atmospheric reflection (88%), and future changes in albedo will likely be primarily due to changes in cloud albedo *(Donohoe and Battisti,2011)*, even small changes in surface albedo can have strong effects: *Donohoe and Battisti* (2011) calculate that the radiative forcing associated with a doubling of CO_2 above preindustrial levels is approximately equivalent to just a 0.01 change in global average planetary albedo. Modeling results of the same study show that, given the extremes in ice and snow cover of the last glacial maximum as compared to an aquaplanet, the changes in planetary albedo are due to nearly equal magnitude contributions from changes in cloud properties and surface albedo. Therefore, knowledge of modified surface albedo in future climates can be very important for quantifying planetary albedo.

The albedo measurements and MODIS validation of our campaign presents a unique dataset to examine snow albedo and remote sensing. Almost all previous MODIS comparisons have used field measurements from shortwave broadband pyranometers (*i.e. Streove,2005; Stroeve,2006; Liang, 2005; Painter,2009; Liu,2009),* whereas we have made spectral measurements, allowing independent validation of each of the MODIS narrowbands in addition to the broadband shortwave product. We have also made daily measurements of snow properties that are controlling albedo variability, which allows an opportunity to provide field evidence of the control of grain size and snow chemistry on albedo. Generally, both grain size and impurity content increase during metamorphism so that snow albedo decreases with time. This relationship has been extensively modeled *(Wiscombe & Warren, 1980),* and has been demonstrated with field measurements of snow grain size *(Grenfell & Perovich, 1981; Grenfell & Warren, 1994).* Measurements of snow grain size with a hand lens or macrophotography are somewhat subjective, because it is difficult to estimate an average grain diameter from snow grains that can be highly nonspherical. The relevant parameter for albedo is the optical grain

radius (a sphere equivalent to the surface area to volume ratio of the snow crystal). This value can be field-measured as specific surface area (SSA, m^2/kg), which is related to the optical grain radius as:

$$\mathrm{SSA} = \frac{\text{surface area}}{\text{volume}\ (\rho_{\mathrm{ice}})} = \frac{3}{\mathrm{r}\ \rho_{\mathrm{ice}}}\ , \qquad (1)$$

where *r* is the optical grain radius, and ρ_{ice} is the density of ice. This study presents measurements of SSA using a Dual Frequency Integrating Sphere (DUFISSS) *(Gallet, 2009)*; however we also made coinciding measurements of SSA using stereology methods with snow samples preserved in DEP (*Matzl, 2010),* that will be a valuable intercomparison dataset for the DUFISSS values. Our campaign has collected the first dataset of coinciding measurements of spectral albedo and snow specific surface area at Summit.

MODIS Daily Snow Albedo Product

The MODIS instrument is on both the Terra and Aqua satellites, which were launched in 1999 and 2002, respectively. These satellites are polar orbiting, and measure emitted terrestrial radiation with 10-14 passes per day over central Greenland.

The MODIS daily snow albedo used in this study is a "blue-sky" product, which includes the effects of anisotropic diffuse illumination, multiple scattering between the surface and atmosphere, and a generalized aerosol optical depth *(Roman, 2010)*. Previous to this algorithm development, products were available as "white-sky" (100% diffuse) or "black-sky" (0% diffuse), and users had to combine these products as simple weighted sums to match the true

diffuse fraction of downwelling solar radiation *(Stroeve, 2005).* This requires an assumption that the directional distribution of sky radiance is isotropic, and that albedo enhancement due to multiple interactions between the surface and atmosphere are approximated within the definition of the diffuse fraction. For solar zenith angles >70° and for optically thick atmospheres with angular variation in the diffuse illumination field, these assumptions can lead to accuracy errors in albedo calculations of a few percent *(Roman, 2010).* These errors have been improved upon with the MODIS algorithm used in this study, which has a stated accuracy of 5% or less for high-quality only albedo retrievals (*Liu, 2009).*

Building an accurate snow BRDF model (Bidirectional Reflectance Distribution Function) is an essential part of this algorithm and enables calculation of hemispheric reflectance from a directional radiance measurement. The BRDF specifies the angular distribution of surface scattering as a function of illumination and viewing geometries at a particular wavelength. The MODIS direct broadcast version of the BRDF/Albedo algorithm uses multiple clear sky views over a 16-day period to reconstruct a generalized snow BRDF which is then applied to the observations on a single day to enable retrieval of a daily surface albedo. When sufficient observations across the viewing hemisphere are not available, a secondary algorithm is used to produce a lower quality daily albedo, which is indicated in all plots. Bandwidths (nm) for the seven MODIS narrowbands and the broadband product used in this study are shown in Table 1.1.

Broadband	***Band 3***	***Band 4***	***Band 1***	***Band 2***	***Band 5***	***Band 6***	***Band 7***
300-5000	*459-479*	*545-565*	*620-670*	*841-876*	*1230-1250*	*1628-1652*	*2105-2155*

Table 1.1. Bandwidths (nm) of MODIS albedo products used in this study.

2. METHODS

2.1 FIELD MEASUREMENTS AND INSTRUMENTATION

2.1.1 Daily Albedo Measurements and MODIS Pixel Locations

Albedo was measured every day at ~1100 AM local time (1300 GMT) between May 16 and July 19, 2011. Measurements were made at four fixed sites, each marked with bamboo and separated by 4-6 m, located ~1km east of the TAWO building in the clean snow sector at Summit Station. The spacing of these sites was chosen to sample the approximate visual scale of variability between drifted and scoured features that were observed during the campaign. Additionally, measurements were made at a fifth "roving" site where profiles of snow specific surface area and density were made in the same spot directly after the albedo measurement, and snow chemistry samples were taken nearby. The roving site was continually moving into clean snow, approaching a distance of ~1 km from the fixed sites by the end of the campaign. This method allows us to monitor the temporal change in albedo at a fixed location, which can then be compared to the albedo of a roving site where the simultaneous changes in snow properties are known.

We compare the albedo time series at this location to the 500-meter resolution MODIS albedo pixel centered on the coordinates of the fixed site. In addition, six MODIS pixels immediately adjacent to the south in the clean air sector are compared to analyze for any possible artificial contamination to the signal at our fixed site, and to provide constraints on the spatial variability of the MODIS signal (Figure 2.1).

Measurements of the fraction of diffuse and direct irradiance were made by taking a ratio of consecutive downwelling measurements, and shading the receptor from direct light on alternate measurements. Tools were field-improvised for this measurement, with an assistant holding a ~20 cm diameter cardboard disc taped to the end of a bamboo pole to block direct sunlight and produce a shadow on the receptor.

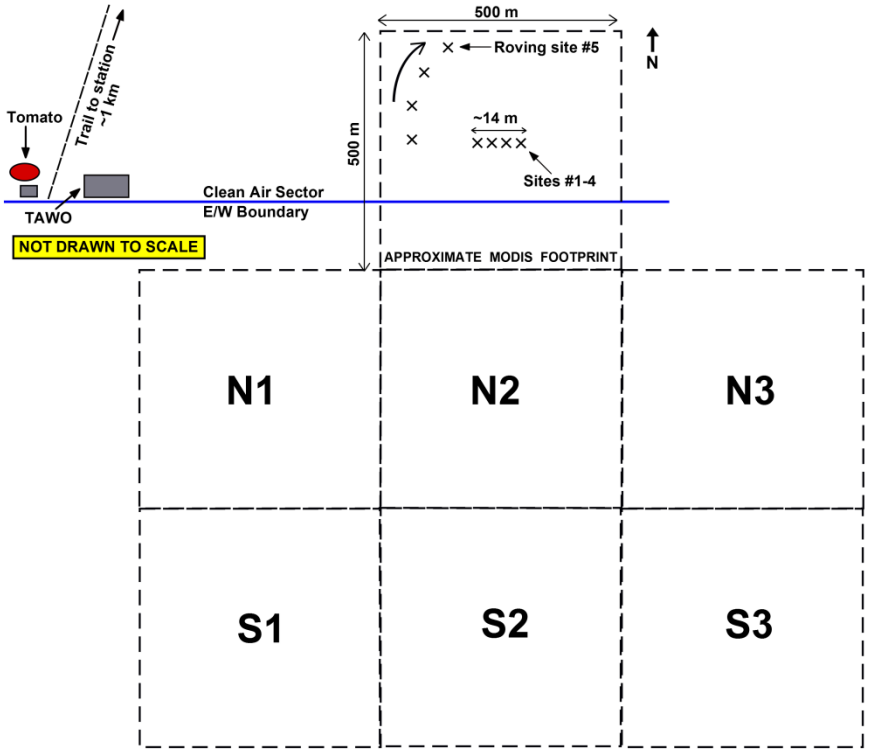

Figure 2.1. Map of the field site at Summit, Greenland, showing the fixed and roving albedo sites and the MODIS pixels used in this study.

2.1.2 ASD Spectroradiometer

Spectral albedo was measured at 350-2200 nm with an Analytical Spectral Devices (ASD) Fieldspec Pro spectroradiometer (2001 model), using the ASD Remote Cosine Receptor (RCR) foreoptic. The cosine receptor was mounted on a 109 cm aluminum arm and held level at approximately 90 cm height by sighting a level bubble on the arm. At this height the cosine receptor has approximately a 2-meter radius field of view for 90% of the signal. Four consecutive albedo measurements were made at every location, enabling an analysis of the precision of the manual leveling technique. This method was found to be more rapid and mobile than the use of a tripod mount, enabling measurements at multiple locations during short time periods (limited by computer electronics in very cold temperatures).

Light entering the cosine receptor travels through a fiber optic bundle to the instrument and is projected onto a holographic diffraction grating where the wavelength components are separated and measured across three detectors. The Visible/Near Infrared detector (VNIR, silicon photodiode array) spans 350-1050 nm at 3 nm spectral resolution. The Short Wave Infrared detectors (SWIR 1 & SWIR 2, indium gallium arsenide (InGaAs)) span 900-1850 nm and 1700-2500 nm, respectively, both at 10-12 nm spectral resolution. The instrument is set to take 40 measurements and 20 dark currents per scan, and digital data from the detectors is transferred directly to a laptop computer which is carried by the user in the field. Measurements are made by standing “down-sun” of the receptor, taking consecutive scans of downwelling and upwelling radiation. Because consecutive measurements are used in ratio to each other in the albedo calculation, irradiance calibration and sensor temperature sensitivity are not applied (instrument last calibrated in 2007).

2.1.3 Spatial and Diurnal Surveys

In addition to the daily surveys, more intensive surveys were made to analyze the spatial and temporal variability of albedo. The spatial surveys were a primary focus for this research, demonstrating the variability that exists within a MODIS pixel, and across multiple pixels. Two long line surveys analyzed km-scale albedo variability on May 17 and June 8, taking measurements every 50 meters moving east along the clean air sector boundary flag line. An additional spatial survey on May 15 analyzed smaller scale albedo variability with measurements every 4 meters on E-W and N-S lines, 32 meters in length. The June 8 survey included snow samples for microtomography analysis, and the May 15 survey included measurements of snow SSA and chemistry.

Diurnal surveys were completed on May 18, 19, and 22. These surveys were "daytime intensives", only measuring albedo between the hours of 1000 and 1700 local time. These surveys show the albedo variability due to changing solar zenith angle, changing diffuse light conditions, and snow crystal growth/metamorphosis throughout the day. These surveys are not analyzed in this thesis.

2.1.4 Snow Physical and Chemical Measurements

Analysis of snow physical properties included specific surface area (SSA), density, and depth profiles of stratigraphy, hardness, and crystal size. SSA measurements were made with a Dual Frequency Integrating Sphere (DuFISSS), operating with lasers at 1310 and 1550 nm *(Gallet, 2009)*. SSA will also be analyzed using stereology analysis of snow samples preserved in DEP*(Matzl,2010)*. Although these data are not presented in this study, it will be used in future publications as an additional SSA dataset. Density profiles were obtained by using a fixed-

volume cutter and a digital scale. Snow chemistry analysis included sampling for ions and elemental and organic carbon, following the methods of Dibb (2007) and Hagler (2007).

2.2 LONG-TERM RADIATION SITES AT SUMMIT (BSRN AND GCNet)

The Baseline Surface Radiation Network (BSRN) site at Summit measures downwelling and reflected irradiance with Kipp & Zonen CM21 pyranometers in the range 305-2800 nm (50% transmittance points), or 335-2200 nm (95% transmittance points), with a maximum reported error of 2% for both hourly and daily totals. These instruments are compliant with ISO 9060 (1990) standards of the World Meteorological Organization (WMO).

The Greenland Climate Network Automatic Weather Station (GCNet AWS) at Summit measures downwelling and reflected irradiance with LI-COR LI-200 pyranometers in the range 400-1100 nm, with a maximum reported error of 5%.

2.3 BROADBAND ALBEDO CALCULATIONS

To compare our measured spectral albedo to the MODIS bandwidths, and to the spectral ranges of the BSRN and GCNet AWS pyranometers, the spectral measurements are integrated over a defined bandwidth, and weighted by the downwelling irradiance. The weighted integral is given by

$$\alpha_{\text{broadband}} = \frac{\int_{\lambda_1}^{\lambda_2} \alpha_\lambda F_\lambda^\downarrow d\lambda}{\int_{\lambda_1}^{\lambda_2} F_\lambda^\downarrow d\lambda}, \qquad (2)$$

where α_λ is the spectral albedo, and $F_\lambda^\downarrow$ is the spectral downwelling irradiance. Because the ASD spectroradiometer was not calibrated for irradiance, we have used an atmospheric radiation model (SBDART) to determine $F_\lambda^\downarrow$ between 350-2200 nm for each day of the campaign at the time of our measurements. Averages of measurements of atmospheric parameters at Summit were used as model inputs. We then compared the model results to measurements from a Biospherical Instruments (BSI) SUV-150B scanning spectroradiometer, at 350-600 nm (0.64 nm resolution, cosine-corrected), located on the roof of the Green House at Summit. Any modeled spectra that had RMSE >0.04 $W/m^2/nm$ were fitted to the BSI spectra by adjusting cloud optical depth on overcast days, or adjusting aerosol optical depth, humidity, and ozone on days when the modeled spectra were less than the measurements. Overall, the model matched the measurements very well (only 3 days out of 52 required fitting) (Figure 2.3). Figure 2.2 shows the seven MODIS bandwidths with a typical clear-sky spectral albedo measurement, and a modeled clear-sky downwelling irradiance spectrum, where the shape of the downwelling curve over the bandwidth dictates the albedo weighting.

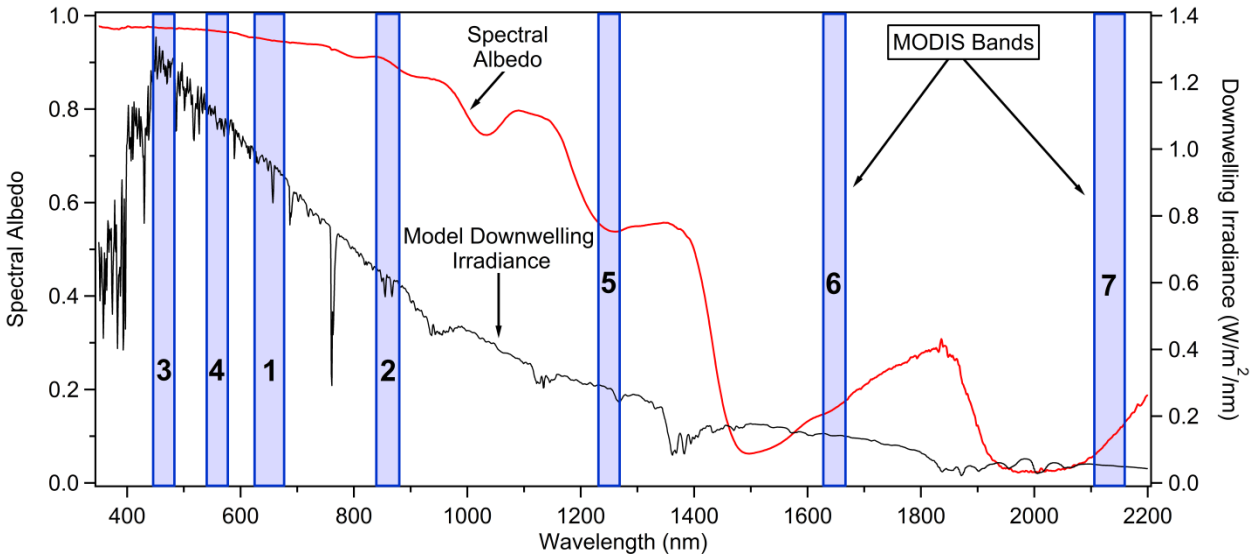

Figure 2.2. MODIS bandwidths shown with a typical clear-sky albedo measurement, and a model downwelling irradiance spectrum.

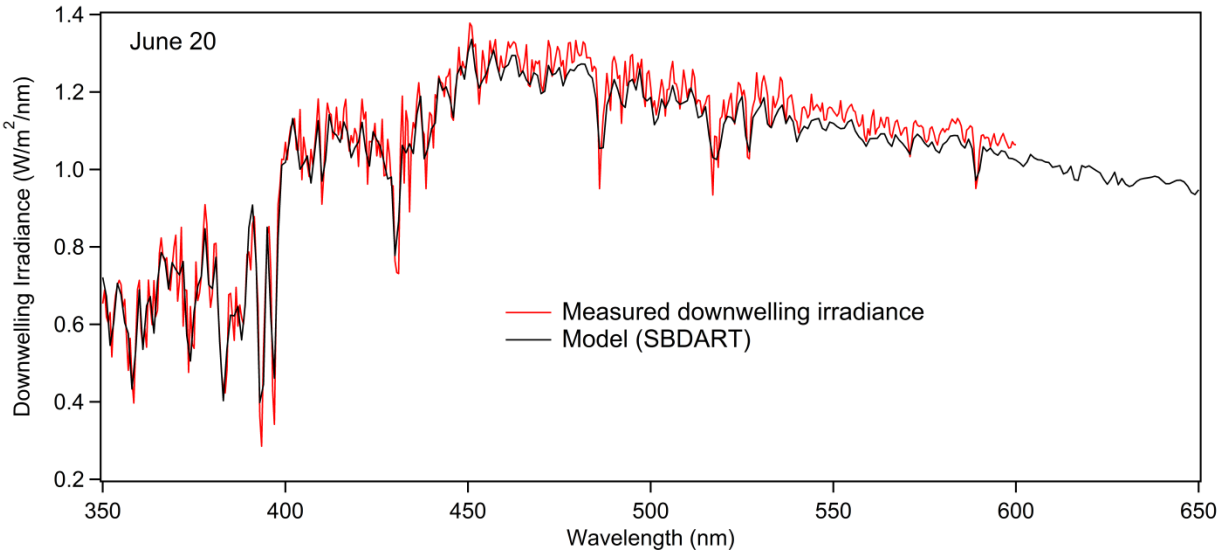

Figure 2.3. Model downwelling irradiance shown with measurements from the Biospherical Instruments scanning spectroradiometer located on the Green House roof at Summit.

2.4 ALBEDO CORRECTIONS, ERROR ANALYSIS, AND QCQA PROCEDURE

2.4.1 Shadow Corrections

Although the ASD operator stands "down-sun" of the receptor to minimize any direct shadowing effects, there is still a shadow produced in the diffuse light field due to the operator. This causes a reduction in the ASD signal for both downwelling and upwelling measurements, thus requiring a calculation of the solid angle of the cosine response volume that is affected by the operator, and a correction factor to increase the measured response.

For clear sky measurements, upwelling reflected radiation is assumed completely diffuse and isotropic, whereas the downwelling has both diffuse and direct components. The measured diffuse fraction of clear-sky downwelling radiation varies with wavelength and is exponentially reduced from ~50% in the UV to almost entirely direct-beam in the long-wave visible and throughout the infrared. Therefore, shadow corrections must be applied independently to the upwelling and downwelling components of diffuse radiation, each calculated as:

$$C_{\text{shadow}\uparrow,\downarrow} = \left(\int_0^{\emptyset}\int_{\theta}^{\frac{\pi}{2}} \sin\theta\cos\theta d\theta d\emptyset\right)\left({}^{1}/_{\pi}\right), \qquad (3)$$

where θ and ∅ are defined by the geometries shown in Figure 2.4. The shadow corrections are then applied to the albedo calculation as:

$$\alpha_{\lambda,\,\text{corrected}} = \frac{C_{\text{shadow}\uparrow}\, F_{\lambda\,(\text{diffuse})\uparrow}}{C_{\text{shadow}\downarrow} F_{\lambda\,(\text{diffuse})\downarrow} + F_{\lambda\,(\text{direct})\downarrow}}, \qquad (4)$$

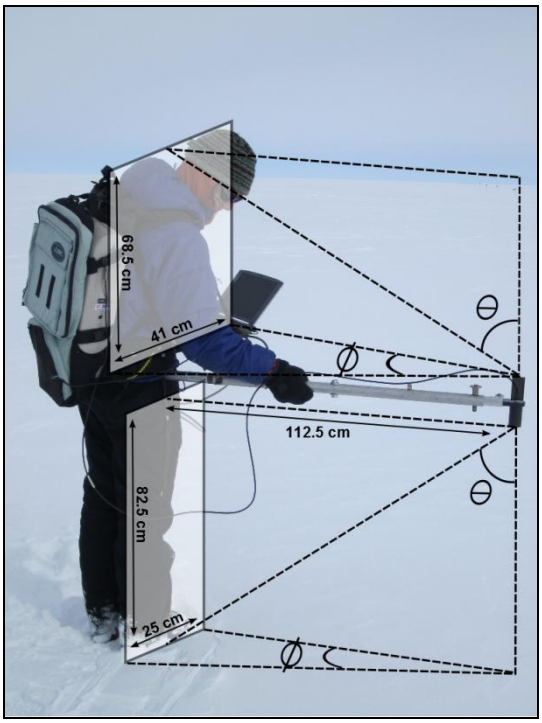

Figure 2.4. Geometries used for calculating the correction due to the shadow of the operator in the diffuse light field.

In addition to the diffuse shadow due to the operator, the projected direct shadow of the instrumentation (aluminum arm + cosine receptor) was also included in the calculation of the correction factor for the upwelling component. The resulting correction factors are0.01552 for the downwelling component, and 0.01310 for the upwelling component. Shadow corrections were not applied to days with consistent overcast conditions, where it is assumed that the diffuse shadow of the upper and lower body approximately offset each other.

2.4.2 Cosine Response Corrections

The response of the ASD RCR receptor deviates slightly from a true cosine response, and corrections for this error should be applied to both the diffuse and direct components. We have attempted to use a laboratory-measured response completed in 2007 for a different RCR receptor

to calculate correction factors (*data from R. Brandt, personal comm., 2012*), but we were unable to calculate realistic values for cosine-corrected albedo (increases to >1.0 in the UV/visible). The procedure used for calculation of cosine correction factors and combined shadow and cosine-corrected albedo are outlined below for reference, but it should be noted that the data used in this study has only been corrected for shadows, and no cosine correction has been applied. All individual spectral albedo curves could potentially increase by an additional ~1% due to the cosine correction, but the RCR receptor used for this fieldwork must be measured for the calculation of an accurate correction.

Using a dataset of measured fractional response as a function of wavelength and incidence angle, the cosine correction factor for diffuse light is calculated following equations fromGrenfell and Warren (1994), as:

$$C_{\lambda,\mathrm{cosine}} = 0.5 / \left\{ \int_0^1 [1 + \varepsilon_\lambda(\mu)]\, \mu \, d\mu \right\}, \qquad (5)$$

where $\mu = \cos\theta$, and ε_λ is the fractional deviation of the measured response from a true cosine response. The final albedo corrected for diffuse and direct cosine response and shadows, is calculated by:

$$\alpha_{\lambda,\mathrm{corrected}} = \frac{C_{\mathrm{shadow}\uparrow}\, C_{\lambda,\mathrm{cosine}} F_{\lambda,\mathrm{diffuse}\uparrow}}{C_{\mathrm{shadow}\downarrow}\, C_{\lambda,\mathrm{cosine}} F_{\lambda,\mathrm{diffuse}\downarrow} + F_{\lambda,\mathrm{direct}\downarrow} / [1+\varepsilon_\lambda(\theta_{\mathrm{sun}})]}, \qquad (6)$$

where $\varepsilon_\lambda(\theta_{\mathrm{sun}})$ is the fractional deviation measured for the incidence angle corresponding to the solar zenith angle of the direct beam. Figure 2.5 shows an example of calculated albedo with shadow corrections (as used in this study), and with cosine corrections (not used in this study, but shown for reference).

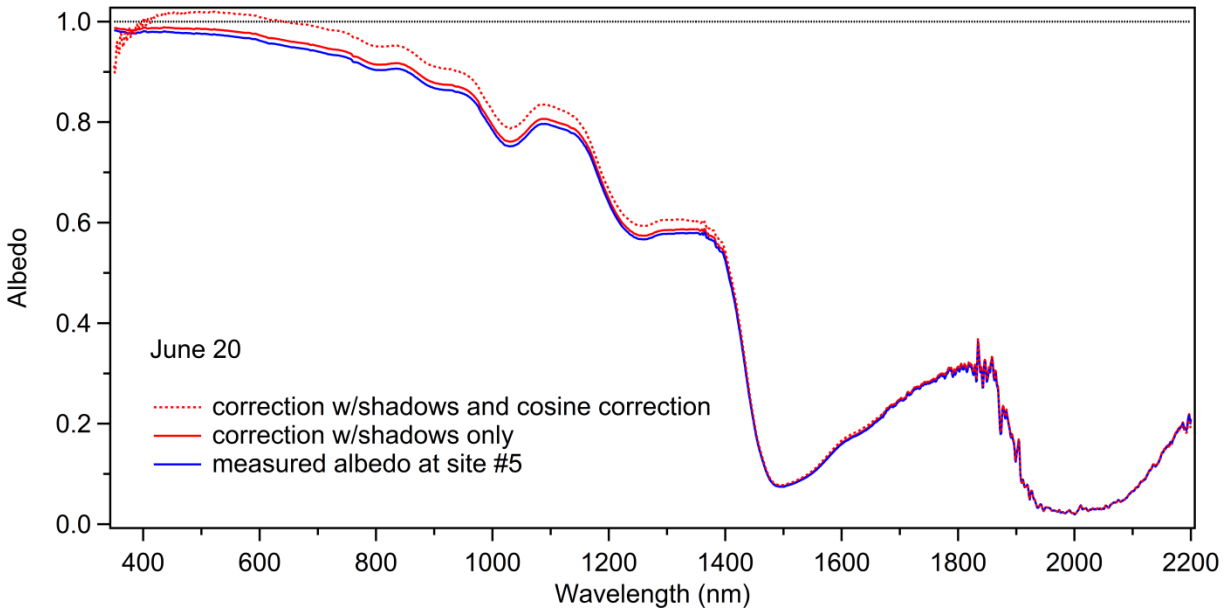

Figure 2.5. Example of spectral albedo calculated with shadow corrections (as used in this study) and with cosine corrections (not used in this study).

2.4.3 Additional Sources of Error

Additional sources of instrumental/operator error that are difficult to quantify but are likely affecting our measurements are: 1) Level of aluminum arm and receptor level. The aluminum arm was leveled visually with a level bubble mounted on both sides, which could result in error due to the inconsistency of the operator's ability to hold level. We tried to achieve high precision of our measurements by completing four consecutive albedo measurements at each site, which gave confidence in the accuracy of the level if the albedo measurements showed high repeatability. Additionally, the cosine receptor mount has two orthogonal level bubbles and is mounted to the arm in such a way that the level between the arm and the receptor can be inconsistent. We would slightly shim the receptor mount in two dimensions to match the level of the arm, but there is certainly some amount of error here that is also attempted to be accounted

for with the precision methods described above. 2) We had multiple operators over the course of the field season, and the changing height and shape of the operators will result in slight errors in the shadow corrections and in the field of view of the cosine receptor. 3) Our instrument has unknown fiber optic cable condition, and has distinct temperature sensitivity of the detectors (especially the VNIR detector, which is addressed in 2.4.5).

Two additional sources of error which are potentially quite important include: 1) Surface roughness (slight slope angles) that are likely causing variability in our measurements as apparent albedo (discussed in detail in Chapter 4), and 2) Seasonal change in solar zenith angle. The solar zenith angle at 1100 local time changes from ~56° at the beginning of the campaign, to 50.7° at the solstice, and then returns to 53.4° on July 19. The effect this change has on our measured albedo has not yet been determined.

2.4.4 QCQA Procedure

The discontinuity present in the final dataset of measured albedo is a result of data reduction from our quality control and quality assurance procedure. Bad data were predominantly a result of inconsistent lighting conditions resulting from passing clouds on days that were not entirely clear or overcast.

There were two rounds of QCQA, identified as "QCQA level-I" and "QCQA level-II". The level-I procedure addressed instrumental error only, whereas level-II addressed error due to sky conditions and inconsistent light. For QCQA level-I, the data on the first VNIR detector (<976 nm) was spliced to be continuous with data on the SWIR 1 detector, if "detector-jump" was greater than 0.005. This problem was quite common in our data, expressed as a distinct

“jump” in signal between the first two detectors, likely a result of temperature sensitivity of the silicon photodiode array on the VNIR detector that results in inconsistent voltage across the detector. It was clear that the relative levels between elements on the array were consistent, and that the problem was due to a change in absolute magnitude across the entire detector, thus justifying a splice of the data to provide a continuous albedo spectrum.

After splicing, albedo spectra were removed that: 1) Plotted >1.0 in the UV/visible; 2) Were obvious outliers from the remaining measurements for a site, that otherwise showed high repeatability (both (1) and (2) are signs of leveling issues); 3) Displayed “parabolic” instrumental error on the VNIR detector (<976 nm). This is another problem that has been documented by ASD, and is also due to the instability of the VNIR detector. (Note that these measurements could often still be used for spectral analysis >976 nm, or for MODIS bands 5,6, and 7, thus resulting in the higher N values for statistical analysis of these bands).

Finally, the remaining albedo measurements for each site were averaged, usually with 3-4 measurements used per site. Because this first round of QCQA paid no attention to sky conditions, any reasonable measurements on cloudy or partly cloudy days were included, and if there was low repeatability across all measurements for a stake (no clear outliers), the measurements were all averaged together if they survived the editing process above.

For QCQA level II, observations including weather field notes, the shape of the diffuse fraction curves, and the signals of nearby buried UV sensors were used to determine the sky conditions at the time of the ASD measurements. Each day with variable sky conditions (not totally clear or totally overcast) was classified as "conditionally good" or "most likely bad". Time series plots were used to focus on days that showed high standard deviation between consecutive measurements, or were large outliers in the time series. Days that showed variable sky conditions

coinciding with large error and/or obvious outlier albedo values, were classified "most likely bad" and were not included in the final dataset. Remaining days that: 1) displayed variable sky conditions (often thin cirrus, haze or diamond dust, or weakly overcast), and 2) still had somewhat repeatable measurements (low standard deviation) and did not produce large outlier albedo values in the times series, were kept as "conditionally good".

It should also be noted that many days did not have measurements at all due to the ASD/laptop having cold-related problems, or due to high winds or other special surveys taking place. After the QCQA procedure, there were approximately 40 days of data remaining (depending on the site and the bandwidths analyzed), out of 65 potential measurement days (May 16 to July 19).

3. RESULTS

3.1 ASD AND MODIS TIME SERIES

Figure 3.1 shows the ASD field-measured albedo time series for all five sites, integrated for MODIS Band 3 (459 – 479 nm), MODIS Band 5 (1230 – 1250 nm), and a broadband integration for the full spectral range of the instrument (350 -2200 nm). An important feature of these plots is the high correlation between the 4 fixed sites and the roving site #5, and the range of variability displayed between all five sites. These bands are shown as representative UV and IR bandwidths, and identical datasets for all five sites have been produced for all MODIS bands through Band 7.

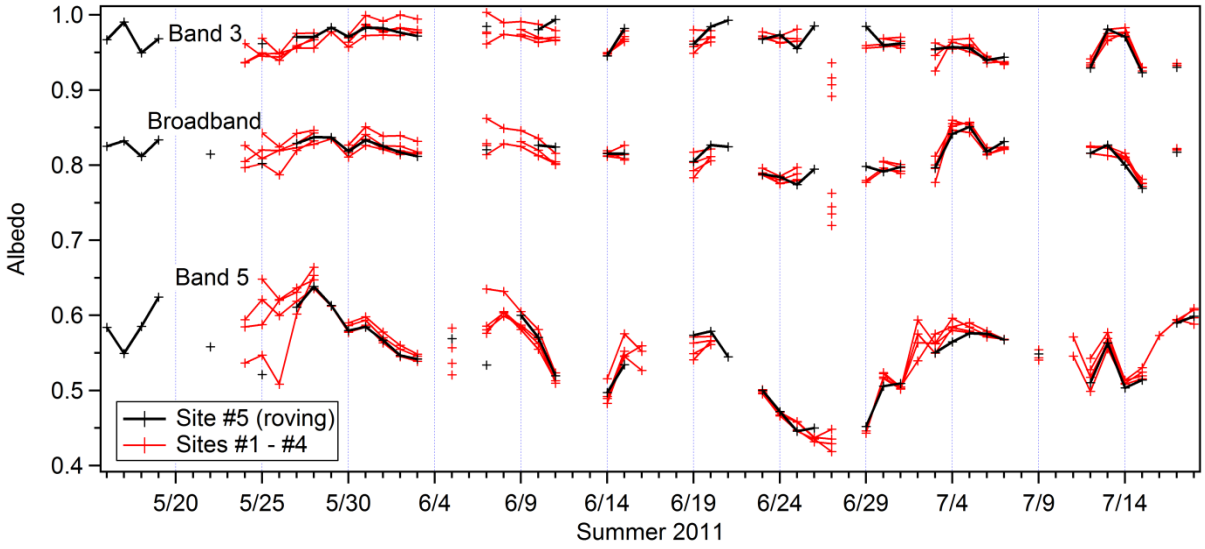

Figure 3.1. Time series of ASD field-measured albedo at all five sites, for Band 3 (459 – 479 nm), Band 5 (1230 – 1250 nm), and Broadband (350 – 2200 nm).

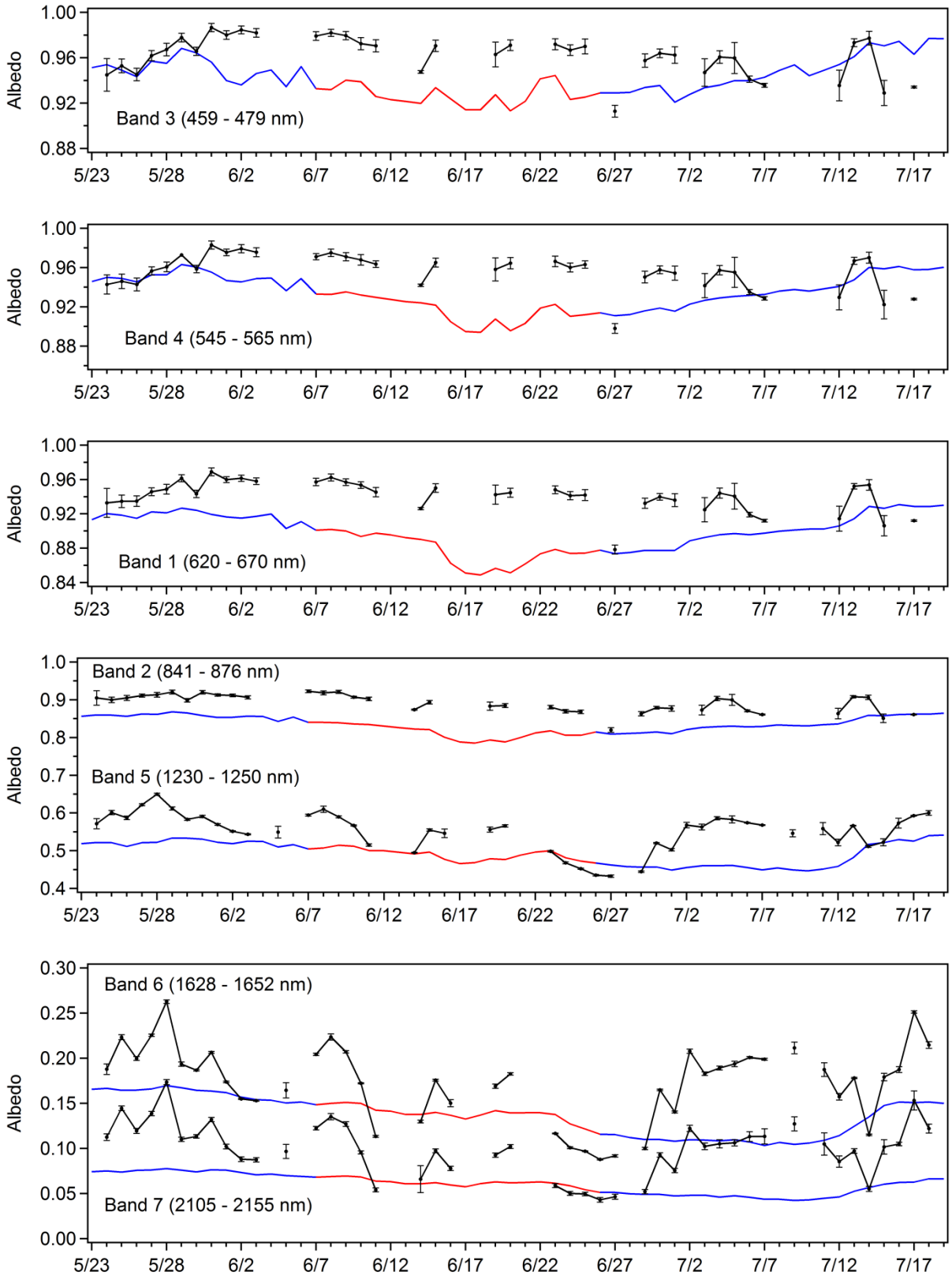
Albedo
Band 3 (459 - 479 nm)
Band 4 (545 - 565 nm)
Band 1 (620 - 670 nm)
Band 2 (841 - 876 nm)
Band 5 (1230 - 1250 nm)
Band 6 (1628 - 1652 nm)
Band 7 (2105 - 2155 nm)
5/23
5/28
6/2
6/7
6/12
6/17
6/22
6/27
7/2
7/7
7/12
7/17

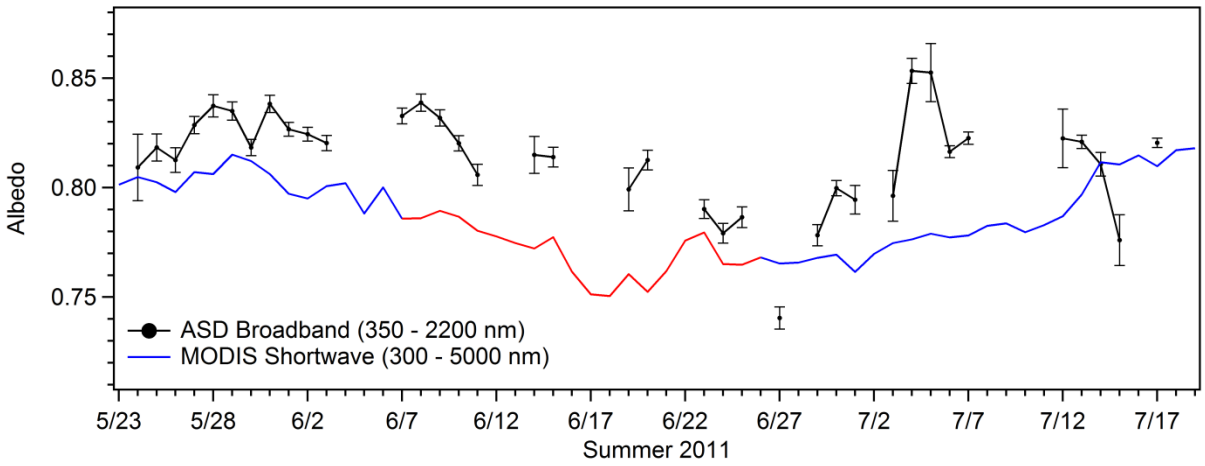

Figure 3.2. Time series of ASD field-measured albedo and MODIS albedo for all MODIS bandwidths. MODIS high-quality data is shown in blue, low-quality in red. ASD albedo is an average of the four fixed sites, with error bars representing the average standard deviation of the four sites, where standard deviation at a single site represents the variability between repeated measurements at that location.

Figure 3.2 shows time series plots of ASD field-measured albedo as an average of the fixed sites #1 -4, with MODIS satellite-measured albedo for all MODIS bandwidths and the MODIS shortwave product. MODIS low-quality flagged data is indicated in red, and high-quality flagged data is indicated in blue. The ASD measurements are discontinuous due to lack of measurements on certain days or from the QCQA procedure described in 2.4.4. The data shown represents the highest quality measurements of the campaign, with many points representing 16 albedo measurements (an average of 4 measurements at all 4 locations). Tables 3.1 and 3.2 show the correlation and error statistics for the ASD and MODIS comparison.

MODIS High-Quality Only

MODIS Band	N (days)	r^2	mean difference	RMSE
Broadband	25	0.136	0.023	0.033
Band 3	25	0.018	0.009	0.024
Band 4	25	0.138	0.010	0.022
Band 1	25	0.170	0.028	0.035
Band 2	25	0.392	0.045	0.050
Band 5	32	0.229	0.063	0.077
Band 6	32	0.138	0.045	0.059
Band 7	32	0.167	0.045	0.052

Table 3.1. Correlation and error statistics for MODIS high-quality only vs. ASD field measurements. Improvement due to high-quality MODIS data is shown in red.

MODIS All Data

MODIS Band	N (days)	r^2	mean difference	RMSE
Broadband	37	0.168	0.027	0.035
Band 3	37	0.004	0.020	0.031
Band 4	37	0.011	0.020	0.031
Band 1	37	0.029	0.040	0.047
Band 2	37	0.277	0.055	0.059
Band 5	45	0.212	0.058	0.073
Band 6	45	0.130	0.037	0.054
Band 7	45	0.141	0.039	0.048

Table 3.2. Correlation and error statistics for all MODIS data vs. ASD field measurements.

3.2 SPATIAL VARIABILITY

3.2.1 ASD Albedo Spatial Variability

The following results are from two approximately 1.5 kilometer transects walking east from the TAWO building along the clean air sector boundary, measuring albedo approximately every 50 meters. The goal of these surveys is to constrain the range of spatial variability, and to compare this variability to the magnitude of temporal albedo variability. The May 17 survey began at 10:41 local time (SZA 55.22°) and ended at 12:12 (SZA 53.08°). The June 8 survey began at 13:47 local time (SZA 50.64°) and ended at 15:31 (SZA 55.29°). Although there are no obvious signs in the data of significant error due to changing solar zenith angle, this certainly has some effect on the measurements and has not yet been quantified. The range and standard deviation of these surveys is shown in Tables 3.3 and 3.4.

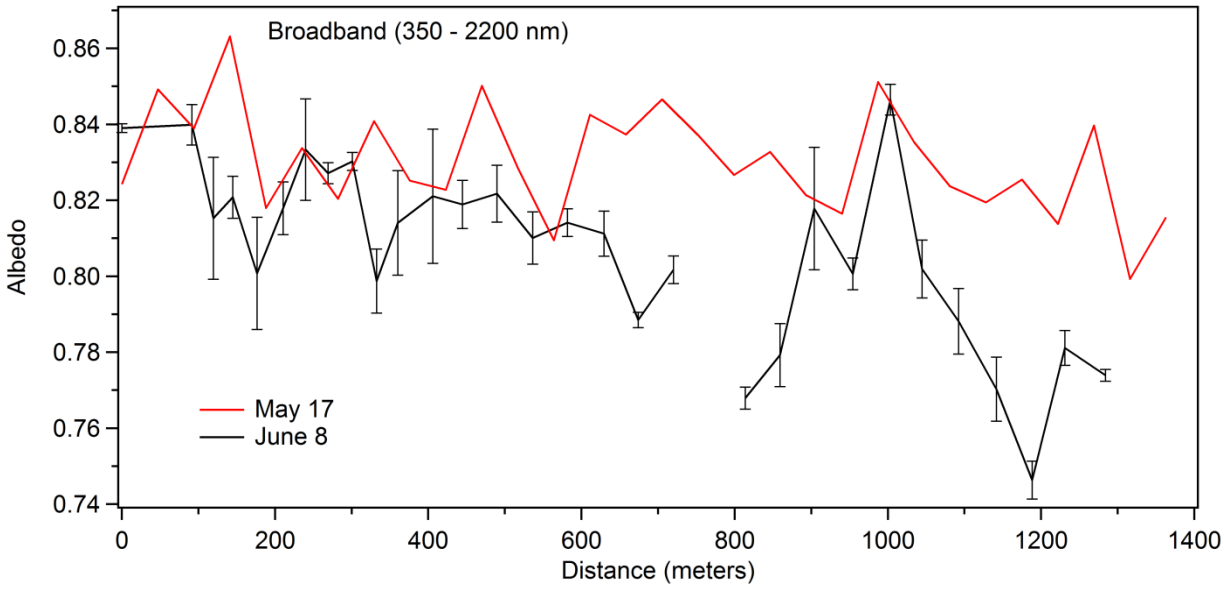

Figure 3.3.ASD broadband albedo measurements from spatial surveys on May 17 and June 8. Measurements are approximately every 50 meters, with one measurement per location on May 17 and 4 measurements per location on June 8 (error bars are 1 standard deviation of the repeated measurements).

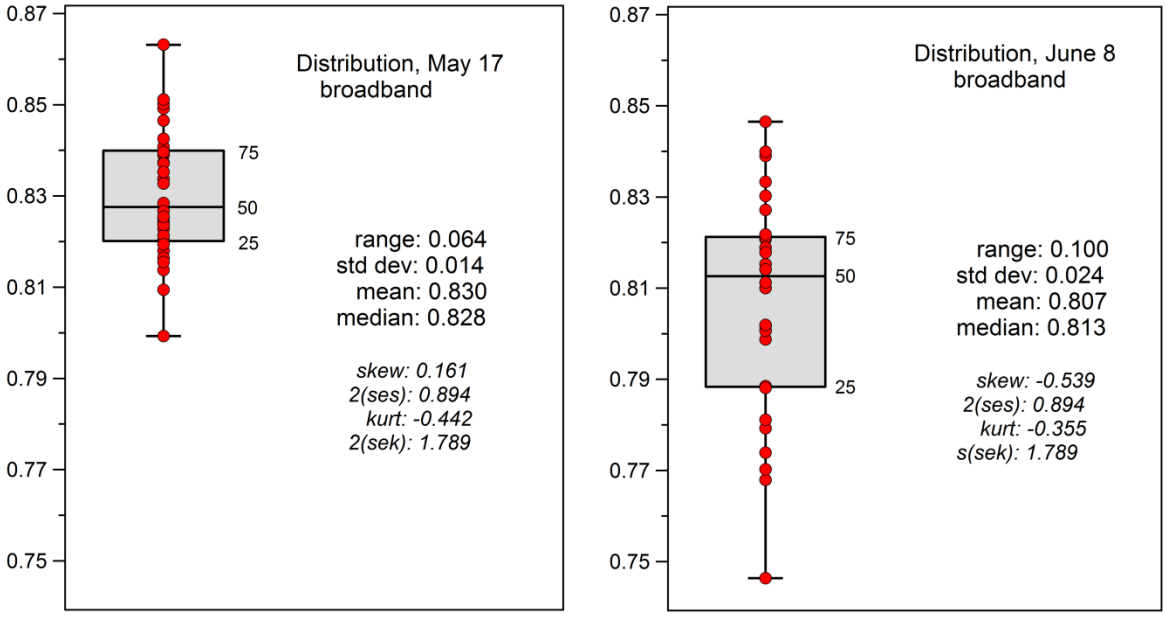

Figure 3.4. Distribution of measurements for the May 17 and June 8 spatial surveys. Boxes indicate quartiles around the median, and whiskers extend to outliers. Both surveys showed distributions that approximate normal.

May 17 Survey	Range	Mean, Std Dev
Broadband	0.064	0.830, 0.014
Band 3	0.057	0.977, 0.013
Band 4	0.068	0.969, 0.014
Band 1	0.071	0.955, 0.015
Band 2	0.075	0.918, 0.017
Band 5	0.087	0.583, 0.022
Band 6	0.048	0.211, 0.012
Band 7	0.032	0.135, 0.008

Table 3.3 Range and standard deviation of the May 17 spatial survey.

June 8	Range	Mean, Std Dev
Broadband	0.100	0.807, 0.024
Band 3	0.118	0.949, 0.024
Band 4	0.133	0.942, 0.028
Band 1	0.135	0.929, 0.029
Band 2	0.119	0.887, 0.030
Band 5	0.084	0.581, 0.023
Band 6	0.035	0.203, 0.009
Band 7	0.017	0.121, 0.005

Table 3.4 Range and standard deviation of the June 8 spatial survey.

3.2.2 MODIS Albedo Spatial Variability

MODIS pixels to the south of the fixed measurement site in the clean air sector were selected as shown in figure 2.1. These additional six 500-meter resolution pixels were analyzed to investigate if the albedo signal of the fixed measurement site was possibly being artificially contaminated by small features such as bamboo, footpaths, or the ASD operator standing in the pixel at the time of the MODIS measurement.

The plots of the additional MODIS pixels did not show any obvious artificial affect in the fixed measurement site pixel that would have caused it to be an outlier to the other pixels. There is a period where the site pixel shows the lowest albedo of the additional pixels, but it is mostly within the range of variability of all the analyzed pixels throughout the study period, and even briefly has a maximum albedo signal. The MODIS narrow bandwidths show similar patterns

among the pixels as the broadband plot. This data is also important for constraining the spatial variability of albedo measured by MODIS at the 500-meter scale.

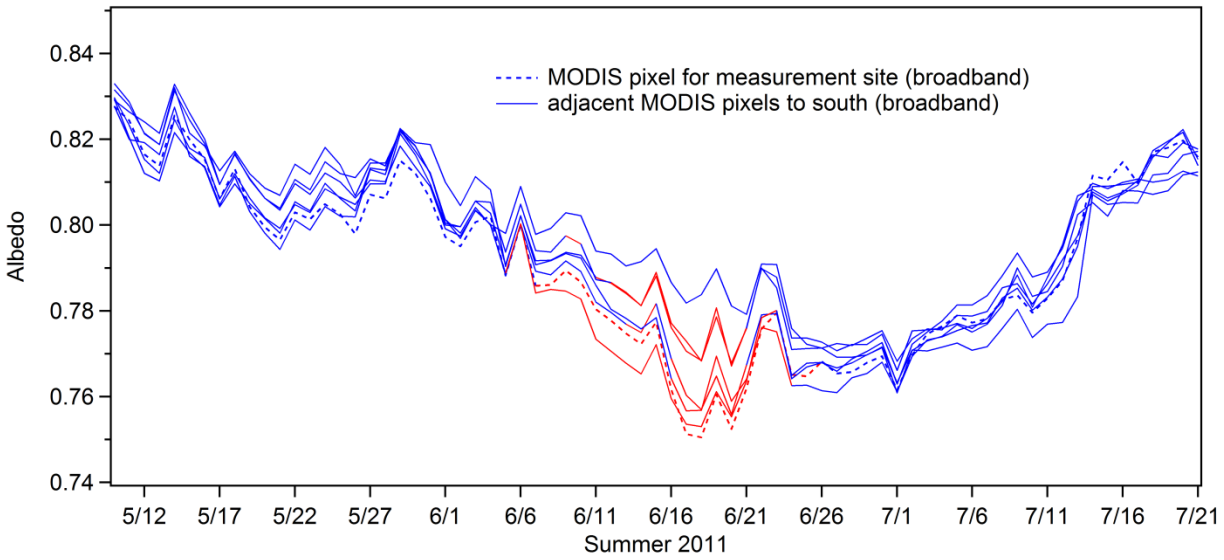

Figure 3.5. Albedo time series for MODIS shortwave product (300 – 5000 nm) for the fixed measurement site (dashed), and for 6 adjacent MODIS pixels to the south in the clean air sector, as indicated in Figure 2.1. Red indicates low-quality MODIS flags.

3.3 BSRN AND GCNet ALBEDO MEASUREMENTS

The Baseline Surface Radiation Network (BSRN) site at Summit provides high-quality data for comparison with both ASD and MODIS albedo. Figure 3.6 shows the albedo time series for all three platforms (*BSRN data from Steffen, personal comm., 2012*), using the ASD and MODIS signals from the fixed-site measurement location. The BSRN site is located ~1 km to the north of the fixed-site location, and a MODIS pixel was not obtained for this location due to the high amount of artificial objects that contaminate the pixel. The ASD measurements are generally in good agreement with the BSRN station at Summit (Table 3.3).

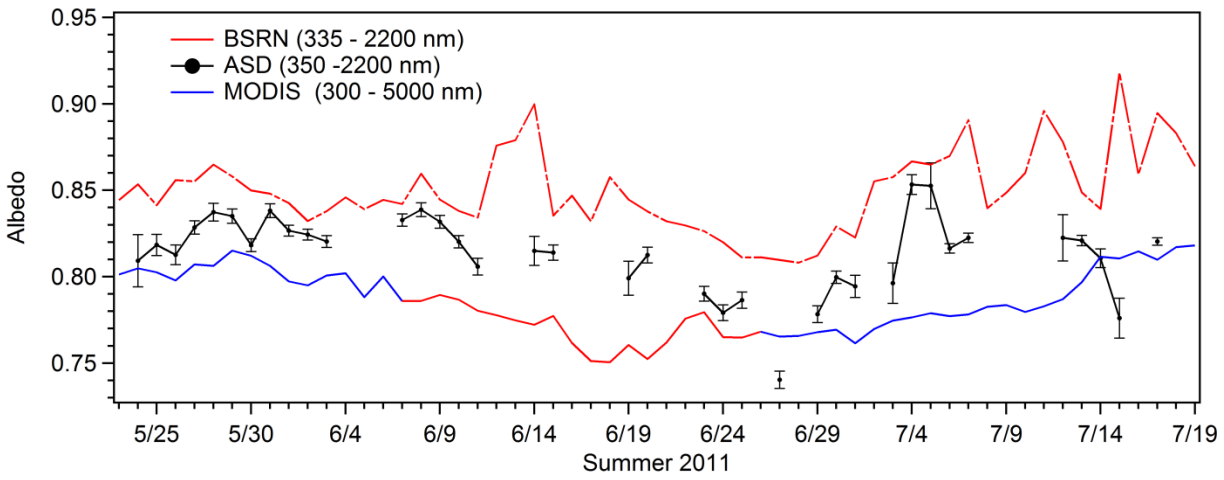

Figure 3.6. Albedo time series for the BSRN station, the ASD broadband integration, and the MODIS shortwave product. Red indicates low-quality MODIS flags.

	N	r^2	mean difference	RMSE
BSRN vs. ASD	37	0.142	0.036	0.045
BSRN vs. MODIS (high quality)	39	0.173	0.060	0.065
BSRN vs. MODIS (all data)	58	0.140	0.065	0.069

Table 3.3. Correlation and error statistics for BSRN vs. ASD albedo, and BSRN vs. MODIS albedo.

A comparison of the ASD and MODIS albedo to the Greenland Climate Network Automatic Weather Station (GCNet AWS) located at Summit presented problems that were not resolved in this study (*AWS GCNet data from Steffen, personal comm., 2011).* A comparison with the GCNet AWS albedo is essential to put our study into context with previous MODIS comparisons, and a preliminary plot is included here for reference (Figure 3.7), although the AWS data is unrealistically low for the instrument wavelength range. The GCNet station operates LI-COR LI-200 pyranometers that measure at 400-1100 nm, and the ASD albedo was

integrated for this wavelength range to produce an equivalent signal, yet the resulting ASD albedo integration is approximately 0.10 higher than the GCNet measurements. A MODIS pixel for the GCNet coordinates was obtained, but the MODIS shortwave data has not been scaled to represent an equivalent wavelength range to GCNet, and thus is not included in Figure 3.7. In previous MODIS field validations the GCNet data is used extensively *(Stroeve, 2005; Stroeve, 2006; Liang, 2005),* and a scaling factor is always applied to the GCNet data to allow equivalent comparison to the wavelength range of MODIS, thus making it difficult to directly compare our GCNet signal to that of previous studies. It should be noted that in previous studies this scaling factor results in AWS albedo values that are very similar to the raw data used in Figure 3.7, thus there is suspicion that the raw data obtained from the AWS for 1100 local time is inaccurate.

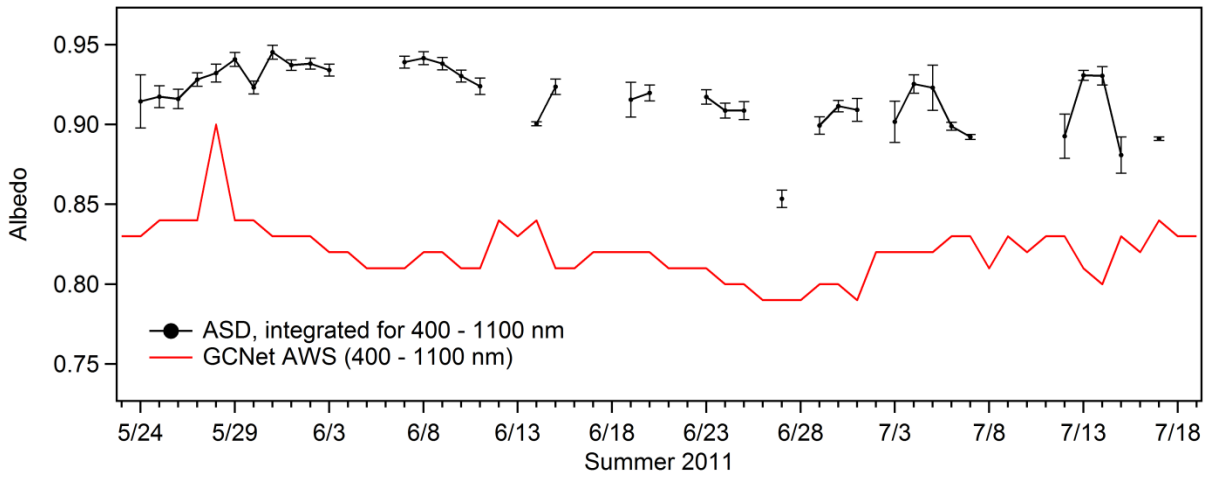

Figure 3.7. Albedo time series of the GCNet AWS station and ASD measurements. ASD data is integrated for the wavelength range of GCNet, yet shows a poor match to the AWS measurements. The AWS values shown are unrealistically low for the wavelength range of the instrumentation, and thus the accuracy of the AWS data is suspected to be poor.

4. DISCUSSION

4.1 COMPARISON TO PREVIOUS STUDIES

All previous MODIS comparison or "validation" studies for the Greenland ice sheet have used data from the Greenland Climate Network Automatic Weather Stations (GCNet AWS), which use broadband pyronometers as described in section 2.2, thus we compare only our broadband integration error results. The mean difference value of our study is equal to, slightly greater than, or sometimes considerably greater than that of previous studies, and the RMSE value of our study is significantly less than most previous studies (Table 4.1).

The lower mean difference and higher RMSE values of previous studies indicate that there are periods with relatively high positive absolute error (AWS albedo > MODIS albedo), but there are often a similar amount of days with negative absolute error (AWS albedo < MODIS albedo), thus the datasets offset each other resulting in low mean difference values, but retaining high RMSE values. This relationship is also visible in many of the time series plots from previous studies. In comparison to these studies, our ASD measurements are consistently higher than MODIS albedo with only two days plotting lower than MODIS, but with lower absolute error. RMSE is a more representative error indicator in the case of previous studies, where the datasets show both positive and negative mean difference (thus the predominance of RMSE as reported in abstracts). The significantly lower RMSE values in our study confirm an improvement from previous MODIS products with the use of the MODIS direct broadcast BRDF/albedo algorithm.

location (year)	N (days)	r^2	mean difference	RMSE	MODIS quality flags	reference
Summit (2012)	25	0.136	0.023	0.033	high only	This study
Summit (2012)	37	0.168	0.027	0.035	all	This study
All stations (16) (2000 – 2003)	--	--	<0.020	0.040	high only	Stroeve (2005)
All stations (16) (2000 – 2003)	~175/yr	--	<0.020	0.070	all	Stroeve (2005)
Summit (2000 – 2003)	--	All-sky/BSA 0.253 All-sky/WSA 0.319 Clear-sky/BSA 0.135 Clear-sky/WSA 0.161	0.027 0.032 0.020 0.025	0.065 0.074 0.061 0.069	all	Stroeve (2005)
Summit (2000 – 2003)	--	--	-0.007 0.003 -0.012 -0.012	--	high only	Stroeve (2005)
All stations (5) (2004)	158	0.624 (Terra) 0.593 (Aqua)	--	0.067 (T) 0.075 (A)	all	Stroeve (2006)
Summit (2004)	~55	--	--	0.035 (T) 0.037 (A)	all	Stroeve (2006)
All stations (5) (2002)	~20	--	<0.02	0.04	all	Liang (2005)
Summit (2002)	~20	--	-0.005	0.036	all	Liang (2005)
San Juans, CO (2006)	30	--	0.036	0.042	all	Painter (2009)

Table 4.1. Correlation and error statistics from this study (broadband integration), and from previous studies using MODIS albedo retrievals over snow (all from the Greenland Ice Sheet except Painter (2009), in Colorado, USA.) MODIS products used include: MOD10A1 and MYD10A1 in Stroeve (2006), MOD43 in Stroeve (2005), DEA in Liang (2005), and MODSCAG in Painter (2009). When the use of MODIS quality flags has not been specifically listed in a previous study, "all" is indicated. "BSA" and "WSA" indicate values reported only for Black Sky Albedo and White Sky Albedo. "T" and "A" indicate the Terra and Aqua satellites. Hash marks indicate unreported data.

4.2 DAILY VARIABILITY VS. SPATIAL VARIABILITY

In section 3.1 the correlation and error is defined for the ASD field measurements and MODIS albedo, but there is also a significant difference in the daily and multi-day range of variability between the two signals, with the ASD measurements showing much higher variability over the course of the campaign (Figure 3.2). In the following section, analyses are made to confirm the variability of the ASD measurements, and to isolate the scale of spatial variability from that of temporal variability.

Perhaps the strongest confirmation of the ASD-measured daily variability is the albedo time series measured by the BSRN station at Summit (Figure 3.6). Analyzing the range, and the mean and standard deviation of ASD albedo and BSRN albedo shows very similar results (Table 4.2). This is significant for the overall campaign goals, as the variability of the BSRN signal in part provided the motivation to investigate the albedo variability and the resulting variability in aerosol radiative forcing. Because the downwelling-weighted wavelength ranges of these two surface-based platforms are very similar (335 – 2200 nm and 350 – 2200 nm, for BSRN and ASD, respectively), this analysis serves as an instrument intercomparison, and confirms both the variability and absolute magnitude of the field-measured albedo.

	Range	mean, std dev
BSRN	0.110	0.849, 0.024
ASD	0.113	0.814, 0.023
MODIS (high only)	0.054	0.790, 0.017

Table 4.2. Comparison of range and standard deviation for BSRN, ASD, and MODIS albedo.

The five long-term measurement sites are essentially small spatial surveys every day, and serve as our largest dataset for spatial variability. There are two distinct scales of albedo variability present in the trends of the five long-term measurement sites: that of daily variability (the day-to-day and multi-day shifts in the 4-site averaged signal), and that of spatial variability, defined by the range of variability between the 4 fixed sites and the roving site (Figure 3.1). This scalar distinction is expressed as a defined range of spatial albedo variability on any given day (represented by sites #1 - 5), that moves through shifts of larger scale variability resulting in the dominant trends of the ASD time series.

The smoothed profile of the MODIS time series could potentially be explained as an "averaging" of a range of meter-scale field-of-view albedo values that exist spatially throughout the 500-meter pixel, where the ASD is simply randomly sampling one of these values each day, and thus could be representing an extreme of the average, resulting in the highly variable plot. However, our combined fixed site and roving site data show that this is not the case. The four fixed sites predominantly range ~2% (standard deviation of ~1%) across all bands, representing 4-6 meter variability over ~14 meters, and the fifth roving site (which moved throughout and beyond the MODIS pixel over the course of the campaign) almost never increases this range (Table 4.3). Therefore, we are measuring albedo that is within ~2% variability for any position throughout the MODIS pixel.

Spatial variability of albedo sites #1-5

	range	mean, std. dev.	range (+ site 5)	mean, std. dev. (+ site 5)
BB	0.019	0.009	0.020	0.009
B3	0.017	0.008	0.019	0.008
B4	0.019	0.008	0.021	0.009
B1	0.020	0.009	0.022	0.009
B2	0.025	0.012	0.027	0.011
B5	0.025	0.012	0.028	0.012
B6	0.011	0.005	0.013	0.006
B7	0.008	0.004	0.009	0.004

Table 4.3. Average range and average mean and standard deviation of spatial variability between the four fixed ASD albedo sites, and the corresponding change in values from adding the fifth roving site.

Table 4.3 shows that there is a defined range of spatial variability that exists across the MODIS pixel at any measurement location, and Table 4.4 shows that the daily variability magnitude is considerably greater than the spatial range. In the broadband time-series, the ASD daily variability ranges 11% for multiday periods, with nearly 6% change present on consecutive days. Bands 3, 4, and 1 range 7-9%, with 5% change present on consecutive days. Longer wavelength bands show even higher variability, with a maximum at Band 5, showing more than 20% variability over the course of the campaign, and a 7.5% change between consecutive days. The range and standard deviation of daily variability of the 4-site averaged albedo and of MODIS is shown in Table 4.4. This daily variability is a defining feature of our field measurements, and is also the most dominant difference between the MODIS and ASD measurements.

Band	range (4-site ave)	range (MODIS high only)	mean, std dev (4-site ave)	mean , std dev (MODIS high only)
Broadband	0.113	0.054	0.814, 0.023*	0.790, 0.017
Band 3	0.074	0.054	0.962, 0.018	0.947, 0.014
Band 4	0.085	0.052	0.956, 0.018*	0.940, 0.015
Band 1	0.091	0.057	0.940, 0.019*	0.906, 0.018
Band 2	0.103	0.059	0.891, 0.024	0.842, 0.019
Band 5	0.217	0.087	0.551, 0.050*	0.490, 0.034*
Band 6	0.175	0.066	0.174, 0.042	0.134, 0.025*
Band 7	0.130	0.035	0.099, 0.030	0.059, 0.013*

Table 4.4. Range and standard deviation of daily variability for the ASD 4-site average and the MODIS high-quality only time series. Asterisks indicate data that is significantly non-normal in distribution.

The two spatial surveys (Figures 3.3 and 3.4) support the variability model presented above, in that there is still a defined range of spatial variability that displays a relative shift from one survey to the next, but these surveys certainly display higher values of range and standard deviation than the five fixed sites (Tables 3.3 and 3.4). While the May 17 survey shows values that are still well below the range of daily variability, the June 8 survey shows range and standard deviation that is similar to the scale of daily variability (with the exception of Bands 5,6, and 7, which still show larger daily variability ranges). Table 4.5 summarizes the distinctions in spatial variability between the long-term sites and the spatial surveys, as well as that of daily variability of the 4-site average.

	spatial w/site 5 (range, std dev)	0517 survey (range, std dev)	0608 survey (range, std dev)	daily var. (range, std dev)
Broadband	0.020, 0.009	0.064, 0.014	0.100, 0.024	0.113, 0.023
B3	0.019, 0.008	0.057, 0.013	0.118, 0.024	0.074, 0.018
B4	0.021, 0.009	0.068, 0.014	0.133, 0.028	0.085, 0.018
B1	0.022, 0.009	0.071, 0.015	0.135, 0.029	0.091, 0.019
B2	0.027, 0.011	0.075, 0.017	0.119, 0.030	0.103, 0.024
B5	0.028, 0.012	0.087, 0.022	0.084, 0.023	0.217, 0.050
B6	0.013, 0.006	0.048, 0.012	0.035, 0.009	0.175, 0.042
B7	0.009, 0.004	0.032, 0.008	0.017, 0.005	0.130, 0.030

Table 4.5. Range and standard deviation of spatial variability for the long-term albedo sites (including site #5), for the two spatial surveys, and for the daily variability of the 4-site average (outlined in red to distinguish from spatial surveys). Means are not included with standard deviations, but can be found in previous tables.

It is somewhat surprising that the fifth roving site does not show the same scale of variability as the spatial surveys, as it approached similar distances away from the four fixed sites, and would be expected to randomly sample values that show a similar range if these spatial surveys represent the general case at Summit. Although the snow surface appears very spatially consistent at Summit, there is a possibility that the spatial surveys on these days simply sampled conditions that were more variable than existed within the MODIS pixel. We would eventually expect to have a spatial survey that showed a more limited variability similar to the fixed sites, or to have larger magnitude variability on some days at the fixed sites, but we do not observe either. The reasons for the different scales of spatial variability between the five long-term measurement sites and the spatial surveys is not clear, although it does seem likely that the reason for spatial

variability at any scale has a large component due to surface roughness (discussed in section 4.2). The evidence supporting the changes in daily variability throughout the MODIS pixel is quite strong from the large dataset of our long-term fixed-site measurements, and an additional spatial survey made on May 15 needs to be analyzed to further constrain the range of spatial variability surrounding the measurement site. An analysis of the third spatial survey will be included in the final journal publication of this study. Additional evidence supporting the range of daily variability shown in the ASD-measured time series is found in the snow physical and chemical measurements.

4.3. MEASUREMENTS OF SNOW PROPERTIES AND MODELED ALBEDO

It has been demonstrated that snow albedo is most sensitive to changes in snow grain size for wavelengths of ~1300 nm *(Gallet, 2009)*. Because snow specific surface area (SSA) was measured using a 1310 nm laser, an analysis was made of the ASD-measured albedo time series at 1310 nm vs. the time series of SSA (Figure 4.1). This analysis demonstrates that our measured variability of daily albedo in the infrared is highly correlated to changes in snow grain size (Figure 4.2), and acts as an independent confirmation of the albedo time series.

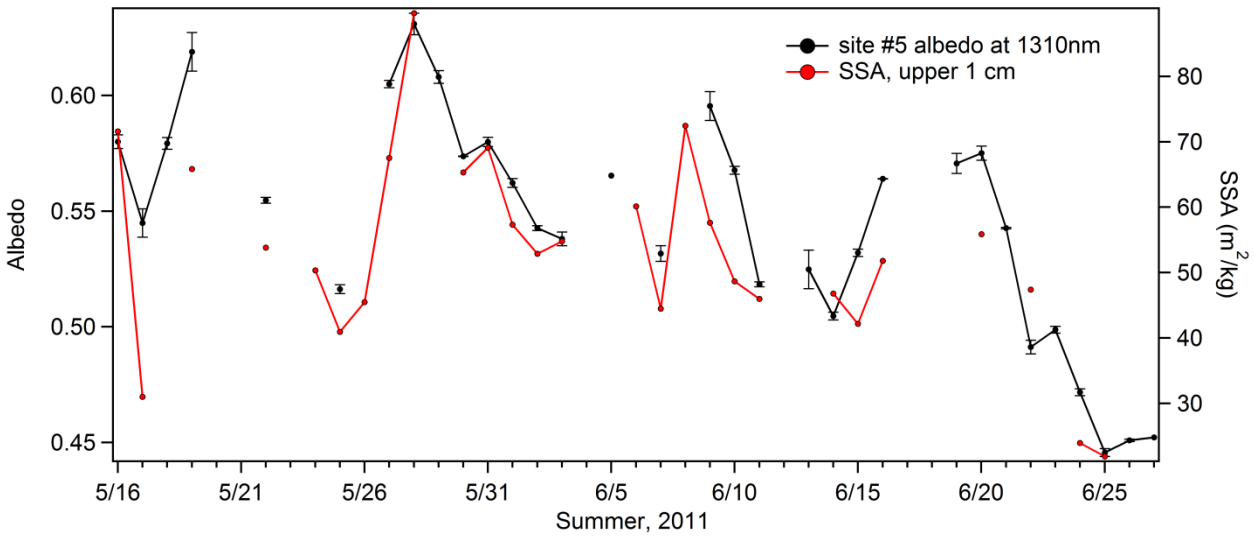

Figure 4.1. Time series of albedo at 1310 nm for site #5, and measurements of snow specific surface area with the DUFISSS instrument.

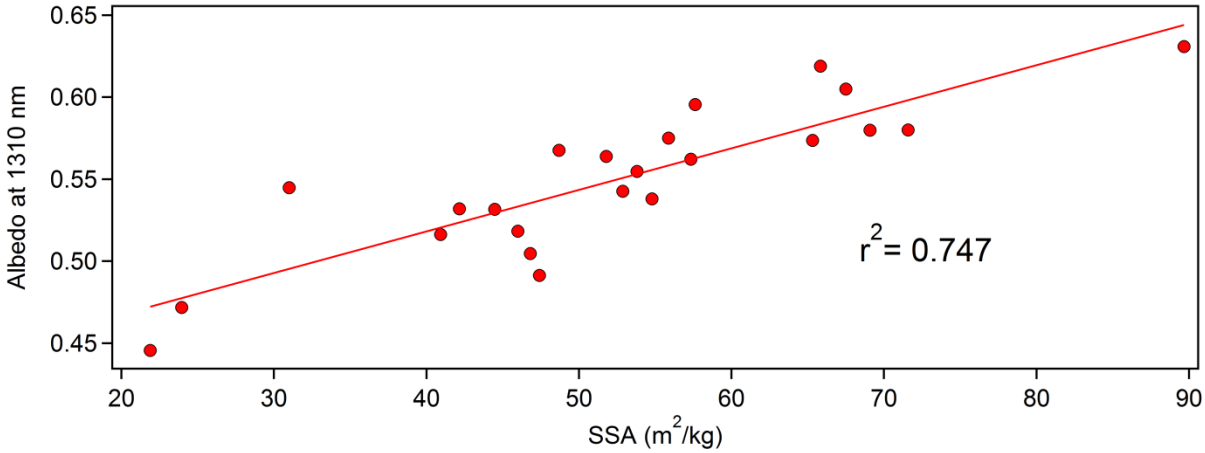

Figure 4.2. Correlation plot of albedo at 1310 nm vs. measurement of snow specific surface area.

Modeling efforts using the DISORT code are being completed by Marie Dumont and Carlo Carmagnola at Meteo-France/CNRS to reproduce daily albedo spectrums using measurements of snow specific surface area, snow density, and elemental carbon measurements. Preliminary results find very good reproduction of the daily measured albedo spectrums, with the difference between modeled and measured albedo generally less than 0.02 (Figure 4.3). These

modeling efforts will be included in future publications from the Summit 2011 campaign, and serve as an independent confirmation of the measured albedo variability.

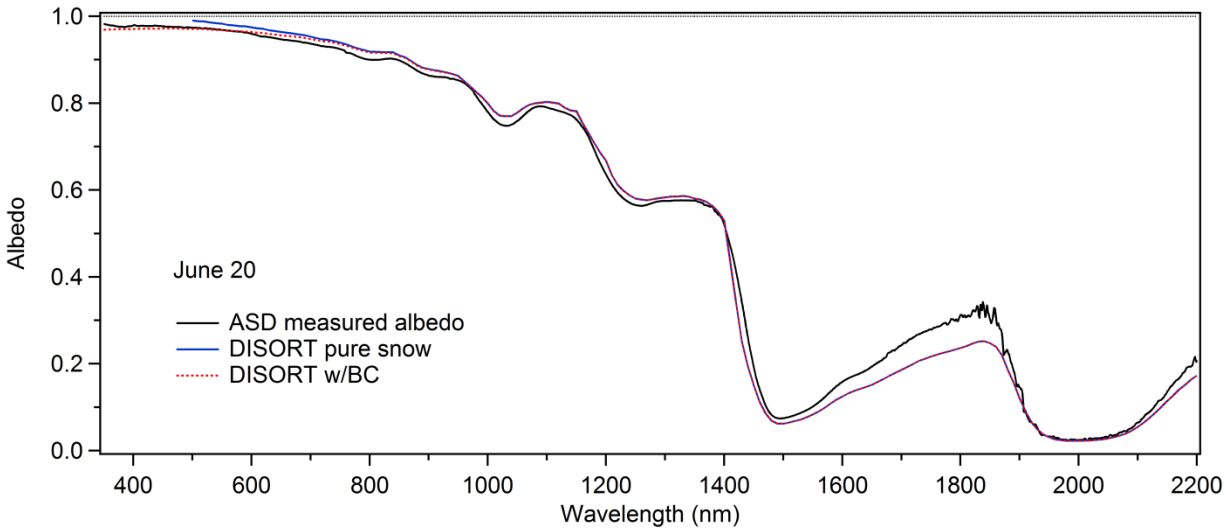

Figure 4.3. Preliminary DISORT model results for June 20, using 3.9 ng/g black carbon. *(Data from Dumont & Carmagnola, personal communication, 2012)*

4.4 SURFACE ROUGHNESS

4.4.1 Possible Effects On Spatial Variability

Any form of surface roughness on the snow has sloping surfaces which can alter the measured albedo under clear skies, resulting in an apparent albedo that is different from the true albedo of the flat surface. Surface roughness and the corresponding magnitude of surface slopes can exhibit many different forms, including features such as sastrugi, suncups, penitents, and simple wind drifts. These features are considered “macroscopic” surface roughness, which is distinct from textural variation resulting from changes in the size and shape of snow crystals,

which can result in kilometer-scale light and dark "banding" effects in the visual scene across the surface of icesheets.

At Summit, the surface roughness in the summer is composed of small wind features that are meters in length and centimeters in height. On Antarctic icesheets, sastrugi fields with heights greater than 0.5 meters are common, however the features at Summit do not resemble these long uniform wave fronts, but rather are randomly distributed wind drifts and scours across an otherwise very flat landscape. This is likely due to the variation in wind direction and speed at Summit, which commonly ranges 180° across the southern sector with occasional shifts to the north, and ranges from calm to gale-force winds. Conditions are usually consistent over the course of a day, resulting in features that are similarly oriented, but the development of uniform sastrugi is prevented with continuous overprinting by new wind features.

For the purposes of the albedo field measurements, it is important to know if our measurements accurately represent the intrinsic albedo of the surface, or if there may be significant error due to upwelling measurements on the sloping flanks of wind features. A study of surface roughness geometry at Summit over a full year in 1998 *(Albert, 2002)* measured the amplitude and wavelength of features that were judged to be characteristic of the surrounding roughness. Summer and fall amplitudes ranged between 3 and 8 cm and had smoothly curved profiles, and wavelengths ranged between 5 and 20 meters. Winter and early spring roughness amplitudes are much greater, but these are not considered as there is minimal solar radiation received during this period. These "wavelengths" are peak to peak measurements of the roughness features and simply represent their spatial distribution, whereas profiles of the individual features show actual lengths of approximately 2 meters. Using this length and an

average amplitude of 5.5 cm, the results of *Albert (2002)* show that, on average, a 3° slope, 1 meter in length, is typically encountered every 5 to 20 meters at Summit during the summer.

During fieldwork in summer 2011, we observed features formed during very high wind conditions that were approximately 10 cm in height, and 500 cm in length, producing slope angles close to 1°. The apparent albedo resulting from slopes of both 3° and 1° are calculated below as if these slopes occupy the entire field of view of the instrument, to demonstrate the maximum effect of a sloped surface. *Grenfell et al. (1994)* present an equation to calculate apparent albedo of a sloped surface:

$$\alpha_\lambda(\mathrm{ap}) = \alpha_\lambda(\mathrm{true}) \frac{\cos[\theta_{\mathrm{sun}} + \theta_{\mathrm{surf}} \cos\varphi]}{\cos\theta_{\mathrm{sun}}} \left[1 - \frac{\theta_{\mathrm{surf}}}{2}\right], \qquad (7)$$

where θ_{sun} is the solar zenith angle, θ_{surf} is the slope of the surface, and φ is the solar azimuth defined as zero when the sun is uphill from the detector. The term including the solar azimuth angle accounts for the projection of the incident irradiance onto a sloped surface and is the dominant effect, and the last term in brackets accounts for the slice in the downward hemisphere that would be filled with snow if the surface were level (at an azimuth of 90° the only effect is due to this slice). *Grenfell et al. (1994)* also measured spectral albedo on a sloped surface and found that the calculated apparent albedos matched the measurements very well up to 1400 nm.

Using equation *(7)* for a 3° and 1° slope, and an albedo measurement from June 20 as the true albedo (solar zenith angle of 50.3°), the solar azimuth is varied in relation to the slope to produce a range of apparent albedos (Figure 4.4). The dominant effect is a reduction of albedo, but there is also a slight increase in albedo experienced in an approximately 90° sector when the sun is downhill of the sensor.

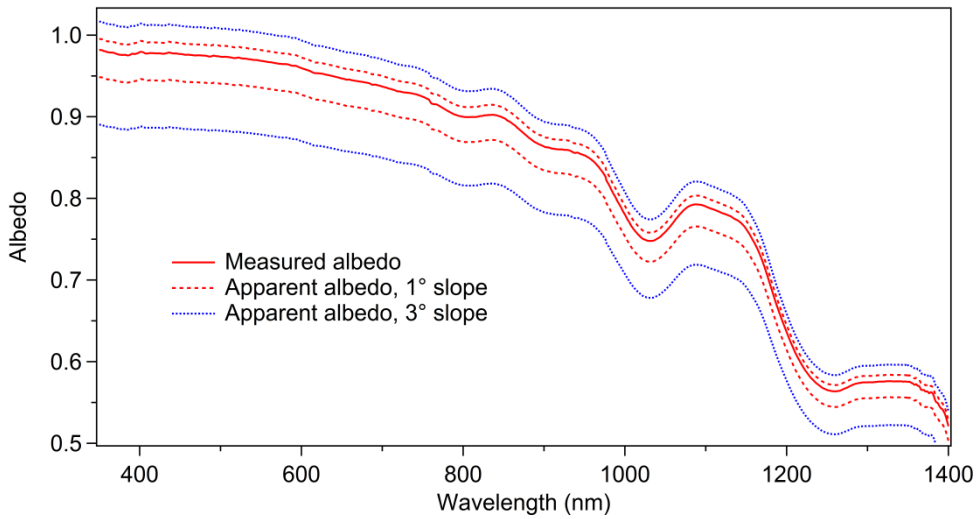

Figure 4.4. Calculated range of apparent albedo due to a sloped surface, after Grenfell and Warren (1994).

The effect of even a small sloped surface is significant: a 3° slope can show apparent albedos ranging from 0.90 (true albedo) to 1.04 (true albedo). The effect of apparent albedo results from the use of downwelling irradiance in the albedo ratio (defined as photons received per unit area incident on a flat surface) which is not equivalent to the irradiance received on a surface tilted away from or towards the sun.

Although the effect of a sloped surface on apparent albedo is large given a consistent surface, the actual effect on our field measurements with the slope angles encountered at Summit is likely smaller. The instrument field of view is approximately 4 meters in diameter, so that the typical 1-meter long sloped surfaces of Albert (2002) will only occupy a fraction of this view, depending on their width in the cross-wind direction. If the features are generally small in relation to the instrument field of view, and are randomly distributed across an otherwise very flat surface, it is unlikely that the upwelling measurements would receive the majority of the cosine response from a significantly sloped or consistently sloped surface. The occurrence of

small slope angles (0.5° - 1°) over longer distances may also be possible, and this could in fact have a larger effect on measurements if the slope occupies the entire field of view. It is difficult to know exactly what the contribution of surface roughness may be to the error of our measurements, with only the end-member calculated scenarios of Figure 4.4.

Some evidence is gained in the spectral signals of the spatial surveys. If the spatial variability was caused primarily by changes in near-surface grain size, then the albedo signal should have largest variability in the infrared surrounding 1300 nm. If surface roughness and issues of relative level were more dominant, then there should be nearly equal variability at all wavelengths according to Equation (*7)* and Figure 4.4. Table 4.5 shows that the latter situation is the case in our surveys, with variability expressed across all wavelengths. This may indicate that surface roughness is a major factor for albedo measurements on the scale of spatial variability, whether in the spatial surveys or for the site to site differences of the four fixed sites. There is evidence that grain size is playing some role, however, in that the exact profile of the variability plot for infrared bandwidths is at times significantly different from the profiles in the UV and visible. This relationship is very clear for the ASD measured albedo time series (Figure 3.2), where the shape of the plot for Band 5 (1230 – 1250 nm) is distinctly different from that of Band 3 (459 – 479 nm) or Band 4 (545 – 565 nm). Additionally, there is a prominent maximum in the range and standard deviation of daily variability at Band 5 (Table 4.5), for both ASD and MODIS albedo. This provides further evidence that the larger scale daily variability cannot be a result of surface roughness alone, and has a strong correlation to changes in snow physical properties.

4.4.2 Possible Effects On MODIS Retrievals

Because MODIS retrievals are directional, the possibility of uniformly oriented surface roughness effecting the satellite measurement must be considered. In the case of large sastrugi and at large solar zenith angles, backscattered radiation is enhanced by altering the angle of incidence, and forward scattering is reduced due to shadows. The effect on bidirectional reflectance patterns is significant, and it is recommended that near-nadir views be obtained for remote-sensing measurements over sastrugi *(Warren et al., 1998).*

However, at Summit the dominant surface roughness is of much lower magnitude and uniformity than the sastrugi fields of Antarctica. The features at Summit tend to be similarly oriented with the current or most recent wind direction (which could cause an effect on the MODIS pixel at a very specific viewing angle), but the features change orientation across the surface on a nearly daily basis as wind directions shift.

The roughness is so subtle at Summit that the only features usually capable of producing shadows near solar noon are very small wind features (centimeters in length and height), that have steep leeward faces and exist as "rippling" on top of the larger meter-scale swells. At the proper viewing angle, some amount of shadowed area may be seen in the MODIS pixel as a result of these features. However, the daily changes in the orientation of the shadowed faces, and the wide variability of view angles of MODIS, eliminate the possibility of directional measurements being consistently altered by this effect. MODIS Terra and Aqua satellites have 10-14 passes over Summit per day, and the albedo algorithm uses multiple clear views over a single day to emphasize that day in the 16-day model, thus incorporating a large range of view angles.

The only element of surface roughness that may be attributable to the consistently lower albedo of MODIS measurements, is large-scale surface topography undulations over distances of 500 meters or greater. These features can have very subtle "shadowing" effects on directional measurements, and would clearly have no effect on the surface measurements. It is common for satellite and airborne albedo measurements to be slighter lower in magnitude than surface measurements *(Stroeve, 2005; Gallet, 2011),* and the optical effects of these long-wavelength surface features is thought to be at least partially responsible for the difference *(Schaaf, pers. comm. 2012).*

There is also a possibility that the 16-day construction of the snow BRDF model in the MODIS algorithm is not capturing daily changes in snow properties, particularly snow specific surface area, and this could explain the lower variability of the MODIS signal. A number of additional atmospheric factors are considered in the MODIS daily albedo algorithm, and could be responsible for error. However, aerosol optical depth over central Greenland is so low that the MODIS error is unlikely related to this parameter in the MODIS algorithm. Assessing the potential for inaccurately modeled variables in the MODIS albedo algorithm is outside the scope of this work, and the reader is directed to Roman (2010) for more information on the details of the algorithm.

5. CONCLUSIONS

The analysis of the ASD field-measured spectral albedo and MODIS albedo time series shows that MODIS albedo is generally lower in magnitude than the ASD measurements, with a broadband RMSE of 0.035 for all days of coinciding measurements, and a broadband RMSE of 0.033 for the MODIS high-quality only retrievals. The MODIS narrowbands show RMSE values (high-quality only) ranging 0.024 – 0.035 in the UV/shortwave visible (Bands 3,4,1), 0.050 in the longwave visible (Band 5), and ranging 0.052 – 0.077 in the near infrared (Bands 5,6,7). These RMSE values are quite low compared to previous MODIS field validations, especially in the UV/shortwave visible region, which comprises most of the solar power spectrum, thus reflecting a similarly low RMSE value for the broadband.

The MODIS albedo does not show similar trends in daily and multiday variability as measured on the surface, resulting in very low correlation coefficients. MODIS albedo displays a more "smoothed" trend over the course of the campaign, whereas the ASD measurements show high variability on day-to-day and multi-day time scales, with the broadband ASD albedo ranging 0.113 over the course of the campaign, commonly with daily shifts up to 0.060. ASD albedo integrated for Band 5 (1230 – 1250 nm) shows the greatest amount of variability, ranging 0.217 over the campaign with daily shifts up to 0.075. This maximum of variability at Band 5 likely represents the effects on albedo of variability in snow specific surface area.

An analysis of our four fixed measurement sites and a fifth roving site shows a defined range of spatial variability that exists throughout the MODIS pixel. Albedo is almost always within 0.02 among all five sites for all bands. The four fixed sites are representative of 4-6 meter variability over a 14 meter distance, whereas the fifth roving site represents measurements up to

a kilometer or more away, and insignificantly increases the range and standard deviation of spatial variability among all five sites. The larger magnitude range of daily and multi-day variability in the time series of the average albedo of the four sites is attributed to changes in surface snow properties that shift as weather and depositional environments change at Summit.

This pattern of daily variability is matched by preliminary modeling efforts which reproduce daily albedo spectra within 0.02 of the measured albedo, using measurements of snow specific surface area, snow density, and snow chemistry (elemental carbon) as inputs to DISORT code. We hypothesize that the error of the modeled albedo is in part due to the error associated with spatial variability of the measured albedo.

The scale of measured albedo variability is also in agreement with the measured range of albedo at the Baseline Surface Radiation Network (BSRN) station at Summit, with range and standard deviation in agreement within 0.003 and 0.001, respectively. There is also relatively good agreement in absolute magnitude with the BSRN station, showing an RMSE value of 0.045, compared to 0.065 for MODIS high-quality only and BSRN albedo.

Two spatial surveys measured albedo approximately every 50 meters on a 1.5 kilometer line, moving east from the four fixed measurement sites. A larger range of variability was measured in these surveys than in the spatial variability of the fixed measurement sites, with one survey showing a similar magnitude of spatial variability to the daily and multiday shifts of the four-site time series. It is likely that surface roughness and error due to apparent albedo is a major component of the variability in these spatial surveys, however further analysis is necessary to resolve the roles of snow grain size vs. surface roughness, and to constrain the range of spatial

variability at Summit. If apparent albedo due to surface roughness can be constrained, this will likely represent a majority of the reported error in our measurements.

This work confirms the variability measured by broadband instruments such as the BSRN station at Summit, which has important implications for the range of direct aerosol radiative forcing over central Greenland. It is also demonstrated that although the MODIS daily albedo product does not capture the range of daily variability as measured on the surface, the MODIS measurements are in better agreement with surface measurements than previous studies, providing increased potential for the use of remotely sensed albedo to aid in calculations of atmospheric and surface processes over the Greenland ice sheet.

REFERENCES

Albert, M. R., and E. F. Shultz (2002), Snow and firn properties and air–snow transport processes at Summit, Greenland, *Atmospheric Environment*, *36*(15–16), 2789-2797.

Albert, M. R., and R. L. Hawley (2002), Seasonal changes in snow surface roughness characteristics at Summit, Greenland: implications for snow and firn ventilation, *Annals of Glaciology*, *35*(1), 510-514.

Brandt, R. E., S. G. Warren, and A. D. Clarke (2011), A controlled snowmaking experiment testing the relation between black carbon content and reduction of snow albedo, *Journal of Geophysical Research*, *116*, D08109, doi:10.1029/2010JD015330.

Dibb, J. E. (2004), Snow accumulation, surface height change, and firn densification at Summit, Greenland: Insights from 2 years of in situ observation, *Journal of Geophysical Research*, *109*, D24113, doi:10.1029/2003JD004300.

Domine, F., A. S. Taillandier, and W. R. Simpson (2007), A parameterization of the specific surface area of seasonal snow for field use and for models of snowpack evolution, *Journal of Geophysical Research*, *112*, F02031, doi:10.1029/2006JF000512.

Domine, F., M. Albert, T. Huthwelker, H. W. Jacobi, A. A. Kokhanovsky, M. Lehning, G. Picard, and W. R. Simpson (2008), Snow physics as relevant to snow photochemistry, *Atmos. Chem. Phys.*, *8*(2), 171-208.

Donohoe, A., and D. S. Battisti (2011), Atmospheric and Surface Contributions to Planetary Albedo, *Journal of Climate*, *24*(16), 4402-4418.

Galbavy, E. S., C. Anastasio, B. L. Lefer, and S. R. Hall (2007), Light penetration in the snowpack at Summit, Greenland: Part 1, *Atmospheric Environment*, *41*(24), 5077-5090.

Galbavy, E. S., C. Anastasio, B. Lefer, and S. Hall (2007), Light penetration in the snowpack at Summit, Greenland: Part 2 Nitrate photolysis, *Atmospheric Environment*, *41*(24), 5091-5100.

Gallet, J. C., F. Domine, C. S. Zender, and G. Picard (2009), Rapid and accurate measurement of the specific surface area of snow using infrared reflectance at 1310 and 1550 nm, *The Cryosphere Discuss.*, *3*(1), 33-75.

Gallet, J. C., F. Domine, L. Arnaud, G. Picard, and J. Savarino (2011), Vertical profile of the specific surface area and density of the snow at Dome C and on a transect to Dumont D'Urville, Antarctica – albedo calculations and comparison to remote sensing products, *The Cryosphere*, *5*(3), 631-649.

Grenfell, T. C. W., Steve G. (1994), Reflection of solar radiation by the Antarctic snow surface at ultraviolet, visible, and near-infrared wavelengths, *Journal of Geophysical Research*, *99*(D9), 18,669-18,684.

Grenfell, T. C., D. K. Perovich, and J. A. Ogren (1981), Spectral albedos of an alpine snowpack, *Cold Regions Science and Technology*, *4*(2), 121-127.

Hagler, G. S. W., M. H. Bergin, E. A. Smith, and J. E. Dibb (2007), A summer time series of particulate carbon in the air and snow at Summit, Greenland, *Journal of Geophysical Research*, *112*, D21309, doi:10.1029/2007JD008993.

Hagler, G. S. W., M. H. Bergin, E. A. Smith, J. E. Dibb, C. Anderson, and E. J. Steig (2007), Particulate and water-soluble carbon measured in recent snow at Summit, Greenland, *Geophysical Research Letters*, *34*, L16505, doi:10.1029/2007GL030110.

Kahl, J. (1997), Air mass trajectories to Summit, Greenland: A 44-year climatology and some episodic events, *Journal of geophysical research. Biogeosciences*, *102*, 26.

Liang, S., J. Stroeve, and J. E. Box (2005), Mapping daily snow/ice shortwave broadband albedo from Moderate Resolution Imaging Spectroradiometer (MODIS): The improved direct retrieval algorithm and validation with Greenland in situ measurement, *J. Geophys. Res.*, *110*, D10109, doi:10.1029/2004JD005493.

Liu, J., C. Schaaf, A. Strahler, Z. Jiao, Y. Shuai, Q. Zhang, M. Roman, J. A. Augustine, and E. G. Dutton (2009), Validation of Moderate Resolution Imaging Spectroradiometer (MODIS) albedo retrieval algorithm: Dependence of albedo on solar zenith angle, *Journal of Geophysical Research*, *114*, D01106, doi:10.1029/2008JD009969.

Matzl, M., and M. Schneebeli (2010), Stereological measurement of the specific surface area of seasonal snow types: Comparison to other methods, and implications for mm-scale vertical profiling, *Cold Regions Science and Technology*, *64*(1), 1-8.

Painter, T. H., K. Rittger, C. McKenzie, P. Slaughter, R. E. Davis, and J. Dozier (2009), Retrieval of subpixel snow covered area, grain size, and albedo from MODIS, *Remote Sensing of Environment*, *113*(4), 868-879.

Román, M. O., C. B. Schaaf, P. Lewis, F. Gao, G. P. Anderson, J. L. Privette, A. H. Strahler, C. E. Woodcock, and M. Barnsley (2010), Assessing the coupling between surface albedo derived from MODIS and the fraction of diffuse skylight over spatially-characterized landscapes, *Remote Sensing of Environment*, *114*(4), 738-760.

Schaaf, C. B., et al. (2002), First operational BRDF, albedo nadir reflectance products from MODIS, *Remote Sensing of Environment*, *83*(1–2), 135-148.

Solomon, S.; Qin, D.; Manning, M.; Chen, Z.; Marquis, M.; Averyt, K.B.; Tignor, M.; Miller H.L. (eds.) (2007), *Climate Change 2007: The Physical Science Basis. Contribution of Working Group I to the Fourth Assessment Report of the Intergovernmental Panel on Climate Change*, 996 pp., Cambridge University Press, Cambridge, United Kingdom and New York, NY, USA.

Stroeve, J. C., J. E. Box, and T. Haran (2006), Evaluation of the MODIS (MOD10A1) daily snow albedo product over the Greenland ice sheet, *Remote Sensing of Environment*, *105*(2), 155-171.

Stroeve, J., J. E. Box, F. Gao, S. Liang, A. Nolin, and C. Schaaf (2005), Accuracy assessment of the MODIS 16-day albedo product for snow: comparisons with Greenland in situ measurements, *Remote Sensing of Environment*, *94*(1), 46-60.

Warren, S. G. W., Warren J. (1980), A Model for the Spectral Albedo fo Snow. II: Snow Containing Atmospheric Aerosols, *Journal of the Atmospheric Sciences*, *37*(12), 2734-2745.

Warren, S. G., R. E. Brandt, and P. O. Hinton (1998), Effect of surface roughness on bidirectional reflectance of Antarctic snow, *J. Geophys. Res.*, *103*(E11), 25,789–25,807, doi:10.1029/98JE01898.

Warren, S. G. B., Richard E.; Grenfell, Thomas C. (2006), Visible and near-ultraviolet absorption spectrum of ice from transmission of solar radiation into snow, *Applied Optics*, *45*(21), 5320-5334.

Warren, S. G., and R. E. Brandt (2008), Optical constants of ice from the ultraviolet to the microwave: A revised compilation, *Journal of Geophysical Research*, *113*(D14).

Wiscombe, W. J., and S. G. Warren (1980), A model for the spectral albedo of snow. I: Pure snow, *Journal of the Atmospheric Sciences*, *37*(12), 2712-2733.